

Parametrization of the Gaussian Disorder Model to Account for the High Carrier Mobility in Disordered Organic Transistors

Yongjeong Lee¹, Sungyeop Jung^{2,3,4,*}, Andrew Plews⁵, Ahmed Nejm⁵, Olivier Simonetti⁶, Louis Giraudet⁶, Sergei D. Baranovskii^{7,8}, Florian Gebhard⁷, Klaus Meerholz⁸, Sungjune Jung^{2,3}, Gilles Horowitz¹ and Yvan Bonnasieux¹

¹LPICM, CNRS UMR 7647, Ecole polytechnique, Institut Polytechnique de Paris, Palaiseau 91128, France

²Future IT Innovation Laboratory (i-LAB), Pohang University of Science and Technology (POSTECH), Pohang 37673, Republic of Korea

³Department of Convergence IT Engineering, POSTECH, Pohang 37673, Republic of Korea


⁴Advanced Institute of Convergence Technology, Seoul National University, Suwon 16229, Republic of Korea

⁵Silvaco Europe Ltd., Cambridgeshire PE27 5JL, United Kingdom

⁶LRN-EA 4682, Université de Reims Champagne Ardenne, 51687 Reims Cedex 02, France

⁷Faculty of Physics and Material Sciences Center, Philipps-Universität, 35032 Marburg, Germany

⁸Department für Chemie, Universität zu Köln, Luxemburger Strasse 116, 50939 Köln, Germany

 (Received 14 September 2020; revised 20 December 2020; accepted 8 January 2021; published 9 February 2021)

Correct parameterization of the Gaussian disorder model (GDM) on spatially random sites is necessary for a complete description of charge transport in disordered materials and concomitant device characteristics. Because the GDM on spatially random sites considers both energetic and spatial disorder, it is superior to the GDM on a cubic lattice. However, analytical arguments and experimental evidence are still lacking for correct parameterization of the model over a wide range of model parameters, energetic and spatial disorder, and electric fields. We show that the model requires a set of parameters to correctly account for high mobility and its charge density dependence, and we develop such a model. The model is implemented in a numerical simulation tool for comparison with the measured device characteristics. Accurate agreement with experimental data, particularly with the high mobility values in organic field-effect transistors, is achieved throughout a wide range of temperature by adjusting both the localization length and the attempt-to-escape frequency.

DOI: [10.1103/PhysRevApplied.15.024021](https://doi.org/10.1103/PhysRevApplied.15.024021)

I. INTRODUCTION

The Gaussian disorder model (GDM) describes charge transport in organic disordered semiconductors (ODSs), such as conjugated polymers [1–8] and small molecules [9–17], as thermally assisted hopping via randomly distributed localized states with the Gaussian density-of-states (DOS) [18–20]. The model accounts for the electric field, charge density, and temperature dependences of charge transport. Therefore, it is adopted for the simulation of organic thin films [21–23], organic diodes [6,24–26], and organic field-effect transistors (OFETs) [6,27,28]. The quality of the model depends on the chosen parameterization and physical assumptions.

Robust parametrization is particularly important for the simulation of OFETs because the operation range of OFETs is wider than that of other applications, covering a full depletion to a strong accumulation regime [29,30]. In

addition, the degree of disorder varies significantly from a crystalline to an amorphous phase. As a consequence, the mobility, which is a concomitant transport parameter, significantly changes in magnitude and in its parametric dependence.

Depending on the assumptions for the spatial distribution of hopping sites, several flavors of GDMs have been developed: GDM on a cubic lattice with off-diagonal disorder (OGDM) [18], GDM on a rigid cubic lattice (EGDM) [19], and GDM on spatially random sites (SRGDM) [20, 31]. The lattice model [19], i.e., the EGDM that considers only energetic disorder, but not spatial disorder, is most widely implemented in numerical simulators [32,33]. The initial parametrization of the EGDM yields a remarkably low mobility of around $10^{-9} - 10^{-15} \text{ cm}^2 \text{ V}^{-1} \text{ s}^{-1}$. Moreover, the core assumptions and parametrization of transport coefficients in the framework of the EGDM are in conflict with well-established results, particularly with respect to field-dependent mobility [34]. Parameters responsible for the effects are not in the EGDM equations, while

*sungyeop.jung@snu.ac.kr

parameters in the EGDM equations are not responsible for the effects [31].

In fact, neither the cubic lattice used so far in device simulations, nor the spatially random sites exploited in our study, can truly represent the realistic amorphous molecular morphology [35]. A spatially random distribution of sites with a given site density can unrealistically lead to two sites being too close to each other or too far from each other. Nevertheless, a system of spatially random sites can be considered as the appropriate model for studying hopping charge transport because of the following reasons.

The coupling of sites with unrealistically small spatial separations in the random model results in very small local resistances, while the coupling of sites with unrealistically large separations results in very large local resistances because of the exponential dependence of the local resistance on the separation between sites. Charge transport is determined by the percolation path, which includes local resistances smaller than the threshold resistance. The latter is the largest local resistance among those that are necessary to provide a connected path through the system. The threshold resistance corresponds to the coupling of sites with separations close to the average separation at a given density [20,31,36]. Therefore, untypically large resistances do not belong to the percolation path, while untypically small local resistances do not contribute to the magnitude of the total resistance.

Furthermore, the absence of the lattice structure in real systems, as evidenced, for instance, by molecular dynamics simulations [35], is of vital importance for the appropriate parametrization of the carrier mobility, i.e., for the topic of our study. As proven by computer simulations [31,37,38], the set of parameters responsible for the physical effects on the lattices is at variance with the parameters responsible for the effects in spatially disorder systems, such as ODSs [31,37,38]. Therefore, the model with spatially random sites should be considered as the appropriate one, compared with the lattice models used so far in the device simulation algorithms.

The model for spatially random sites developed by Baranovskii and co-workers, i.e., SRGDM, proposed a solution of GDM in terms of the transport energy [20,31,39] valid for any steeply energy-dependent DOS, including the exponential DOS and the Gaussian DOS. At low electric field, the mean time of upward hopping rate toward the transport energy from states below the transport energy determines the carrier mobility. At high electric field, the concept of the effective temperature is adopted to describe charge transport [34,40]. The model is more rigorous than the lattice model due to the simultaneous consideration of energetic and spatial disorder. In addition, it could be more robust than the EGDM thanks to a simpler parametrization process. However, a numerical simulation has not been conducted at a device level, especially on OFETs.

Moreover, experimental validation with a variety of ODSs is lacking.

In this study, we present a physical parametrization of the SRGDM, which we consider more realistic for the experimental situation than the lattice models. First, we examine the model parameters related to the mobility and elucidate the relationship between them. Then, to conduct a numerical simulation at the device level, we implement the SRGDM in a technology computer-aided design (TCAD) simulation tool, ATLAS, from Silvaco [41]. The validation of this procedure is performed by comparing the simulation with experimental data of transfer characteristics, measured at various temperatures, of a variety of OFETs fabricated from different types of ODSs. We determine a set of model parameters, including the localization length and the attempt-to-escape frequency, that reflect a genuine transport characteristic of each material.

In Sec. II, we compare the SRGDM and the EGDM in terms of the parametrization method. In Sec. III A, we investigate the limit of the initial parameterization through a literature survey of the field-effect mobility values and the degree of disorder of current OFETs. Then, we show the superiority of the SRGDM over the EGDM by direct comparison of the two models at low electric fields in Sec. III B. To establish a set of parameters, we extract the localization length and attempt-to-escape frequency from various OFETs and examine their validity in Secs. III C and D, respectively. Finally, the choice of this set of parameters is justified by the good agreement between experimentally measured transfer curves of various OFETs and the corresponding numerical TCAD simulation in Sec. IV.

II. THEORY

A. Gaussian density-of-states and Miller-Abrahams (MA) hopping

Principal assumptions of the standard GDM [18] are the Gaussian DOS and the MA hopping transition rate. The Gaussian DOS is expressed as

$$g(\varepsilon) = \frac{N_0}{\sigma\sqrt{2\pi}} \exp\left(-\frac{\varepsilon^2}{2\sigma^2}\right), \quad (1)$$

where N_0 is the total molecular density and σ is the Gaussian width. The MA hopping transition rate is the frequency of hopping of a charge carrier from an occupied state, i , to an unoccupied state, j ,

$$v_{ij} = v_0 \exp\left(-\frac{2r_{ij}}{a} - \frac{\varepsilon_j - \varepsilon_i + |\varepsilon_i - \varepsilon_j|}{2kT}\right), \quad (2)$$

where a is the localization length of a charge carrier; r_{ij} is the distance between sites i and j ; ε_j and ε_i are the energies of initial and final states, respectively; k is the Boltzmann constant; and T is the temperature. The prefactor v_0 is the

attempt-to-escape frequency, typically in the range of 10^{12} to 10^{13} s^{-1} [20,42]. The parametrization of the GDMs is associated mainly with the four physical parameters of an ODS, N_0 , σ , a , and v_0 , in Eqs. (1) and (2). According to the specific model, additional parameters can be considered. The effect of temperature and carrier density is dominant over that of the electric field in OFETs due to the weak lateral field in the channel. Thereby, we focus on the parameters related to temperature and carrier density.

B. SRGDM

The basic idea of this model is that charge-carrier hopping occurs around the transport energy, ε_t , situated in the Gaussian DOS [39,43]. The charge carriers below ε_t hop upwards, and the carriers above ε_t hop downwards, converging to ε_t . In this model, physical parameters determine the mobility directly without a fitting process (Fig. 1).

First, the Fermi level, ε_F , is estimated by the Gauss-Fermi integration for given carrier concentration p . Then, the transport energy, ε_t , for a certain carrier density in the Gaussian DOS is determined by [39]

$$\frac{2}{3} \left(\frac{4\pi}{3B_c} \right)^{-1/3} \frac{kT}{a} \left[\int_{-\infty}^{\varepsilon_t} [1 - f(\varepsilon, \varepsilon_F)] g(\varepsilon) d\varepsilon \right]^{-4/3} \times [1 - f(\varepsilon_t, \varepsilon_F)] g(\varepsilon_t) = 1, \quad (3)$$

where $f(\varepsilon, \varepsilon_F)$ is the Fermi function, and the percolation constant $B_c \approx 2.732$ accounts for the percolation nature of hopping transport [44]. The validity of ε_t is confirmed by a simulation based on the Monte-Carlo method [45]. Subsequently, from knowledge of ε_F and ε_t , one can calculate the hopping distance $r(\varepsilon_t)$ by

$$r(\varepsilon_t) = \left[\frac{4\pi}{3} \int_{-\infty}^{\varepsilon_t} g(\varepsilon) [1 - f(\varepsilon, \varepsilon_F)] d\varepsilon \right]^{-1/3}. \quad (4)$$

The above mathematical formulation considers spatially random sites.

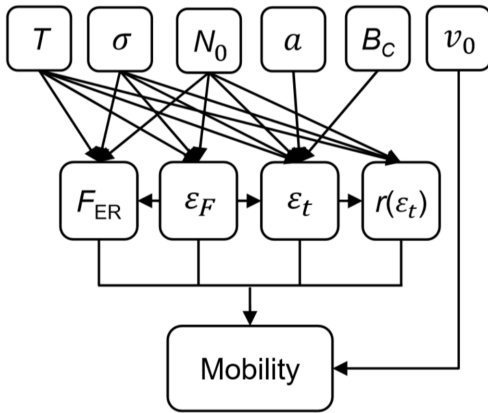


FIG. 1. Parametrization process of the SRGDM.

The carrier mobility can be calculated with the generalized Einstein relation by [20,39]

$$\mu \simeq \frac{e}{kT} F_{\text{ER}} \frac{r^2(\varepsilon_t)}{t}, \quad (5)$$

where F_{ER} is the dimensionless function for generalized Einstein relation [46], e is the elementary charge, and t is the average upward hopping time for all states below ε_t [47,48]. The average time t neglects the downward-hopping transition rate because the downward-hopping transitions are exponentially faster than the upward-hopping transitions [Eq. (2)]. Finally, by using Eqs. (4) and (5), the carrier mobility at the low electric field of the SRGDM becomes

$$\mu \simeq v_0 \frac{e}{kT} \frac{3B_c F_{\text{ER}}}{4\pi r(\varepsilon_t) p} \exp \left[-\frac{2B_c^{1/3}}{a} r(\varepsilon_t) - \frac{\varepsilon_t - \varepsilon_F}{kT} \right]. \quad (6)$$

C. EGDM

The mobility of the GDM on a cubic lattice, i.e., EGDM, at low electric field is the following function of T and of the carrier density p :

$$\mu(T, p) = \mu_0(T) \exp \left[\frac{1}{2} (\hat{\sigma}^2 - \hat{\sigma}) (2pb^3)^\delta \right], \quad (7)$$

where $\hat{\sigma} = \sigma/kT$ is the reduced width of the Gaussian DOS, $b = N_0^{-1/3}$ is the lattice constant, and $\delta \equiv 2[\ln(\hat{\sigma}^2 - \hat{\sigma}) - \ln(\ln 4)]/\hat{\sigma}^2$ [19]. Here, $\mu_0(T)$ is the T -dependent zero-carrier mobility, which has the form

$$\mu_0(T) = \mu_0 c_1 \exp(-c_2 \hat{\sigma}^2), \quad (8)$$

where $\mu_0 = b^2 v_0 e / \sigma$, and c_1 and c_2 are adjustable parameters. Initially, the parametrization of c_1 and c_2 is carried out by fitting Eq. (7) to the numerical simulation result of the master equation, assuming nearest-neighbor hopping (NNH)

$$\sum_{j \neq i} [v_{ij} p_i (1 - p_j) - v_{ji} p_j (1 - p_i)] = 0. \quad (9)$$

Here, p_i is the probability of charge occupation on site i . Based on this method, the initial parametrization of the EGDM is $c_1 = 1.8 \times 10^{-9}$ and $c_2 = 0.42$ at $N_0 a^3 = 10^{-3}$ [19].

On the other hand, in this work, we extract c_1 and c_2 by direct fitting of the reduced mobility of the zero-carrier limit, $\mu'_{\text{red}}(0)$, from Eq. (8), $\mu'_{\text{red}}(0) = c_1 \exp(-c_2 \hat{\sigma}^2)$, to the same from the Vissenberg-Matters (VM) model with the Gaussian DOS [42] (Fig. 2). We adopt the VM model to consider variable-range hopping (VRH), which is an advancement from the initial parameterization and simulation based on Eq. (9) that consider only the first and

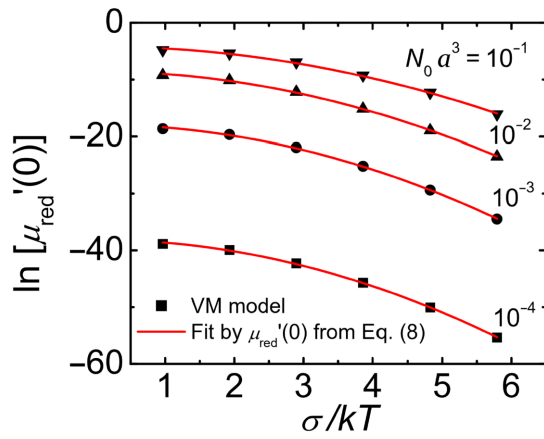


FIG. 2. Reduced mobility $\ln[\mu'_{\text{red}}(0)]$ fitting between numerical solution of the VM model (black dots) and analytical expression from Eq. (8), $c_1 \exp(-c_2 \hat{\sigma}^2)$ (red lines) at $N_0 a^3 = 10^{-1}$, 10^{-2} , 10^{-3} , and 10^{-4} .

second NNHs [49]. The parametrization results of the EGDM are $c_1 = 1.54 \times 10^{-2}$, 1.86×10^{-4} , 1.62×10^{-8} , and 2.75×10^{-17} and $c_2 = 0.35, 0.44, 0.49$, and 0.51 for $N_0 a^3$ values of 10^{-1} , 10^{-2} , 10^{-3} and 10^{-4} , respectively.

In our theoretical considerations, we do not take into account possible correlations between spatial disorder and energetic disorder. We follow, in this respect, the conclusion of Pasveer *et al.* [19], who claim that their theoretical analysis of the field-dependent carrier mobility in polymers such as poly[4'-(3,7-dimethyloctyloxy)-1,1'-biphenylene-2,5-vinylene] (NRS-PPV) and poly(2-methoxy-5-(3',7'-dimethyloctyloxy)-*p*-phenylene vinylene) (OC₁C₁₀-PPV)

does not indicate that there is a need to assume spatial energy correlations. A similar conclusion, at least with respect to the PPV-based materials, was suggested by Bouhassoune *et al.* [50]. There are indications that, while the spatial energy correlations can play an essential role in small-molecular ODSs, such correlations might be not significant for polymers, where the GDM can serve as an appropriate model [51]. In our study on poly[2,5-bis(3-alkylthiophen-2-yl)thieno(3,2-*b*)thiophene] (PBTTT), indacenodithiophene-*co*-benzothiadiazole (IDTBT), and pentacene, we neglect the spatial energy correlations.

III. RESULTS AND DISCUSSIONS

A. Limits of initial parameterization

Before elucidating the parameterization of the GDM, let us first review experimental data on the gate voltage, V_{GS} , dependence of mobility measured from OFETs [1–17,52–54] with various degrees of disorder [55–64] in the literature. In Fig. 3(a), each symbol marks the maximum mobility (μ_{max}) and the order of μ modulation with V_{GS} of a device. The former indicates μ at the maximum $|V_{GS}|$ and the latter indicates how many times μ_{max} increases from μ at the minimum $|V_{GS}|$ within the on state. The transistors fabricated from SC molecules [52–54] and DA copolymers [1–3] exhibit a negligible or very small μ modulation between one and two. On the other hand, the transistors consisting of PC molecules [9–17], semi-C polymers [1,4,5], and disordered polymers [6–8] show a large μ modulation between 5 and 15. In essence, the gate voltage, V_{GS} , dependence of the mobility is strongly correlated

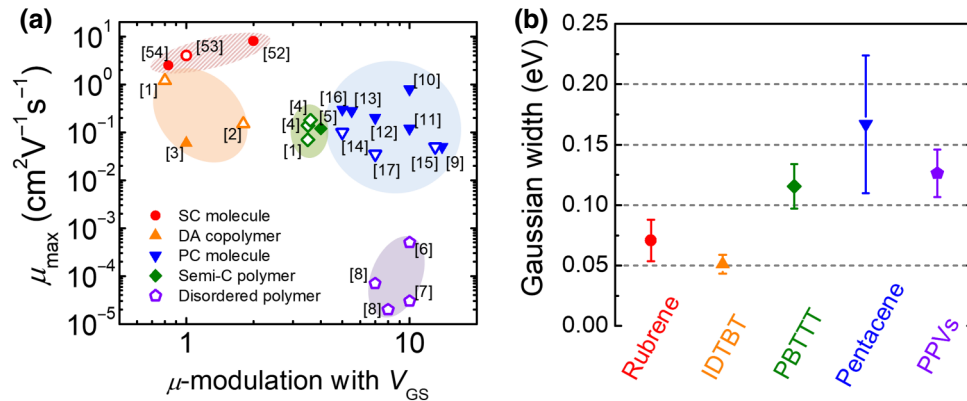


FIG. 3. (a) μ_{max} versus μ modulation with V_{GS} for various OFETs at room temperature. Donor-acceptor (DA) copolymer for IDTBT [1] and poly[2,5-(2-octyldodecyl)-3,6-diketopyrrolopyrrole-alt-5,5-(2,5-di(thien-2-yl)thieno[3,2-*b*]thiophene)] (DPP-DTT) [2,3]; semicrystalline (SemiC.) polymer for poly(3-hexylthiophene-2,5-diyl) (P3HT) [4] and PBTTT [1,5]; disordered polymer for chemically modified PPV [6–8]; polycrystalline (PC) molecule for T6 [9], pentacene [10–15], 5,11-bis(triethylgermylethynyl)anthradithiophene (diF-TEG-ADT) [16], and dihexylsexithiophene (DH6T) [17]; single-crystal (SC) molecule for rubrene [52–54]. Hatched area in red illustrates SC molecules employing bandlike transport, and other shaded areas illustrate materials employing hopping transport. Also, filled symbols represent contact-resistance-corrected μ and open symbols represent contact-resistance-uncorrected μ . (b) Gaussian widths extracted from the literature for rubrene [22,55,56], IDTBT [1,57], PBTTT [1,58,59], pentacene [60–63], and PPVs [6,19,64].

with the type of semiconductor material, in terms of both μ_{\max} and the order of μ modulation with V_{GS} . The aim of this study is to explain the “thermally activated” hopping transport observed in the high-carrier-mobility disordered organic semiconductor, which is opposite to the bandlike charge-transport mechanism SC molecules [65].

In the frame of the GDM, modulation of the mobility with charge-carrier concentration increases when the disorder increases. An identical μ modulation is expected with V_{GS} because applying V_{GS} increases the charge-carrier concentration in the channel. Accordingly, a device exhibiting a large μ modulation with V_{GS} corresponds to a more disordered semiconductor film. Figure 3(b) gives the Gaussian widths of a representative material for each category defined in Fig. 3(a) taken from the literature. When the Gaussian width, σ , which represents the energetic disorder, is small ($\sigma < 0.1$ eV or $2-3kT$ at 300 K), like in IDTBT [1,57], μ modulation is arithmetic by a few times [19,66]. When the Gaussian width, σ , becomes larger ($\sigma > 0.1$ eV or from $3kT$ up to $6kT$ at 300 K), like in PBTTT [1,58,59], pentacene [60–63], and chemically modified poly(*p*-phenylene vinylene)s (PPVs) [6,19,64], μ modulation is exponential by a few orders of magnitude for $\sigma = 3kT, 4kT, 5kT$, and $6kT$.

Although IDTBT, PBTTT, and pentacene are all presumed to be crystalline materials, they often provide evidence of an essential amount of disorder. For instance, Venkateshvaran *et al.* [1] measured the amount of energetic disorder in films of conjugated polymers going from semicrystalline to disordered morphologies and found that semicrystalline PBTTT exhibited an even higher energetic disorder than that of a structurally highly disordered IDTBT copolymer. Estimates for energetic disorder in PBTTT and IDTBT of 47 and 33 meV, respectively, indicate that these materials are disordered organic semiconductors. Polycrystalline pentacene contains structural disorder, as do all polycrystalline semiconductors.

Remarkably, the initial parameterization of the GDM assumes a small localization length a ($a \approx 0.1$ nm) [19,67] in order to describe the characteristics of the transistors with molecularly doped polymers [18] and chemically modified PPVs [19], showing low mobility in the range of 10^{-5} – 10^{-4} $\text{cm}^2 \text{V}^{-1} \text{s}^{-1}$ with μ modulation by about one order of magnitude [6,21]. For this initial parameterization of the EGDM, a small localization length a is decisive in accounting for the low mobility. In fact, most previous studies adopted very small values of a . For instance, $a = 0.2b$ was used in the work by Bäessler [18] and $a = 0.1b$ was adopted by Pasveer [19]; each value corresponds to $a \approx 0.14$ nm for Bäessler’s work and $a \approx 0.07$ nm for Pasveer’s work when $b \approx 0.7$ nm ($b = N_0^{-1/3}$ and $N_0 = 3 \times 10^{21} \text{cm}^{-3}$).

However, this initial parameterization is not adequate in the case of the high mobility values in the range of 10^{-2} – $10 \text{cm}^2 \text{V}^{-1} \text{s}^{-1}$ with similar and/or large μ

modulation about one order of magnitude or larger, as recently observed in transistors with semicrystalline polymers (e.g., P3HT and PBTTT) and small molecules (e.g., pentacene and diF-TEG-ADT). As demonstrated Sec. III B, if the same initial parameters are used, the calculated mobility is several orders of magnitude smaller than the measured one. This means that the charge carrier can hardly hop when the state is strongly localized, i.e., small a , so that the hopping transition rate decreases exponentially by Eq. (2). Recent Monte-Carlo simulation results have also shown that the modification of a significantly changes the mobility [37]. Therefore, in a system with higher disorder, increasing a becomes necessary to set the calculated mobility to the same level as its experimental value.

In addition, the attempt-to-escape frequency, ν_0 , which is the prefactor of the MA transition rate of Eq. (2), also affects the mobility. Common values used in the initial parameterization of EGDM [19,20] are taken from the phonon frequency, 10^{12} – 10^{13}s^{-1} [68,69], with regard to charge-carrier transfer, as the emission or absorption of a phonon abides by the conservation of energy law [70]. This means that ν_0 can vary, depending on the material’s properties, such as the electron-phonon coupling strength, the density of states of phonon, and hence disorder [71]. Therefore, a further study on the relationship between ν_0 and mobility is also a timely subject to improve the consistency of parameterization.

B. Advantages of the SRGDM

To support the need for higher localization length, as claimed in Sec. III A, and to show the advantages of the SRGDM, we calculate the mobility and hopping distance given by the EGDM and that by the SRGDM. For the calculation, we vary the localization length as $N_0 a^3 = 10^{-3}$, 10^{-2} , and 10^{-1} , assuming a fixed N_0 and Gaussian widths of $\sigma = 0.05$ and 0.15 eV (Fig. 4). The difference between the two approaches at high electric field has been already analyzed by Baranovskii and co-workers [37,38]. Here, we show that the difference exists even at low electric field, so the SRGDM is, in general, a better theoretical framework, and parameterization is more necessary for the SRGDM.

Regarding the effect of the Gaussian width, μ modulation with a relative hole density of p/N_0 is negligible for $\sigma = 0.05$ eV, whereas it amounts to about 10^3 for $\sigma = 0.15$ eV, regardless of the localization conditions. In addition, the mobility decreases significantly in the order of 10^{-4} , 10^{-5} , and 10^{-6} for each localization condition, when the Gaussian disorder varies from $\sigma = 0.05$ to $\sigma = 0.15$ eV. Regarding the effect of localization length, the mobility increases significantly by 10^7 for $\sigma = 0.05$ eV and by 10^{10} for $\sigma = 0.15$ eV, when $N_0 a^3$ increases from 10^{-3} to 10^{-1} . This means that the magnitude of μ changes more significantly by a at higher σ . On the contrary,

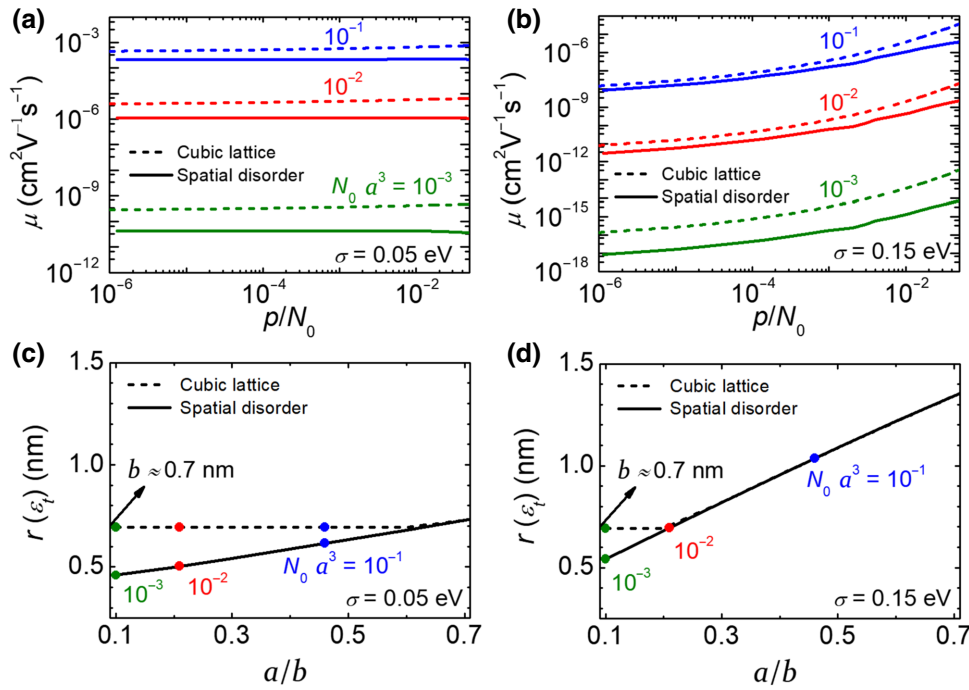


FIG. 4. Mobility calculated by EGDM (solid line) and SRGDM (dotted line) with various $N_0 a^3$ and calculated $r(\varepsilon_t)$ in the cubic lattice and spatial disorder for (a),(c) $\sigma = 0.05$ eV and (b),(d) $\sigma = 0.15$ eV. In the calculation, $\nu_0 = 10^{12}$ s $^{-1}$, $B_c = 2.735$, and $N_0 = 3 \times 10^{21}$ cm $^{-3}$ are used.

the way the modulation of μ is changed by the hole concentration is not affected by the value of a .

Remarkably, the mobility calculated by the EGDM is higher, at least 2.5 times, to about an order of magnitude, than that by the SRGDM, and this tendency is greater for small localization lengths. Concomitantly, the aforementioned variation by Gaussian width or localization length is even more pronounced in the SRGDM. The variation of a covers the transition between two different hopping mechanisms: the charge carriers tend to hop to adjacent states when a is small (NNH), whereas they tend to hop to farther states when a is large (VRH). The discrepancy in mobility between the two GDMs [Figs. 4(a) and 4(b)] results predominantly from the overestimation of hopping distance $r(\varepsilon_t)$ on a cubic lattice under the NNH regime, which is limited to the inter-site distance b [42] [Figs. 4(c) and 4(d)].

For this reason, parameterization for the GDM is necessary and becomes even more important for the SRGDM, to correctly describe charge transport through both VRH and NNH. It is now clear that the modulation of the mobility by hole concentration is determined by the Gaussian width, and the magnitude of mobility is determined by the localization length. In particular, the localization length must be set higher than its conventional values to explain the high mobility in recently reported organic transistors.

C. Localization length

Compared with the mobility measured from OFETs made of DA copolymers, semicrystalline polymers, and polycrystalline small molecules (Fig. 3), the mobility

calculated by the SRGDM using initial parameterization is still too low [Figs. 4(a) and 4(b)]. In order to address this discrepancy, localization length a needs to be enlarged to greater than the values in Fig. 4. The appropriate value of a for each considered material can be determined from the Arrhenius plot of temperature-dependent mobility. Indeed, the activation energy, ε_a , of this plot depends on a by considering that ε_a is the energy that a charge carrier should overcome to hop upwards from the Fermi level, ε_F , to the transport energy, ε_t ($\varepsilon_a = \varepsilon_t - \varepsilon_F$). Here, we note that the localization length a affects ε_t directly, according to the parameterization scheme in Fig. 1 and Eq. (3), while ε_F is independent of a .

Using the SRGDM, we compare the experimentally measured and numerically calculated Arrhenius plot of mobility as a function of the localization length a for various materials, e.g., D-A copolymer (IDTBT, experimental data from Ref. [1]), semicrystalline polymer (PBTTT, experimental data from Ref. [1]) and polycrystalline molecule (pentacene, measured data) [Fig. 5(a)]. The calculation considers a from 0.1 to 1 nm and ν_0 for each a ; ν_0 is determined by fitting to the mobility at the highest temperature. Slopes became smaller as a increased for all materials [Fig. 5(b)]. From the experimentally measured slopes, $\Delta_{\text{exptl.}}$, we obtain $a = 0.75$ nm ($\Delta_{\text{exptl.}} = 48.1$ meV) for IDTBT, $a = 0.29$ nm ($\Delta_{\text{exptl.}} = 137.5$ meV) for PBTTT, and $a = 0.56$ nm ($\Delta_{\text{exptl.}} = 199.4$ meV) for pentacene. Interestingly, the calculated slopes that are regarded as ε_a are smaller than those directly calculated by $\varepsilon_a = \varepsilon_t - \varepsilon_F$ using Eq. (3) [Fig. 5(c)]. This indicates that the slope, Δ , of the empirical Arrhenius form, $\mu(T) \simeq \mu_0 \exp(-\Delta/kT)$

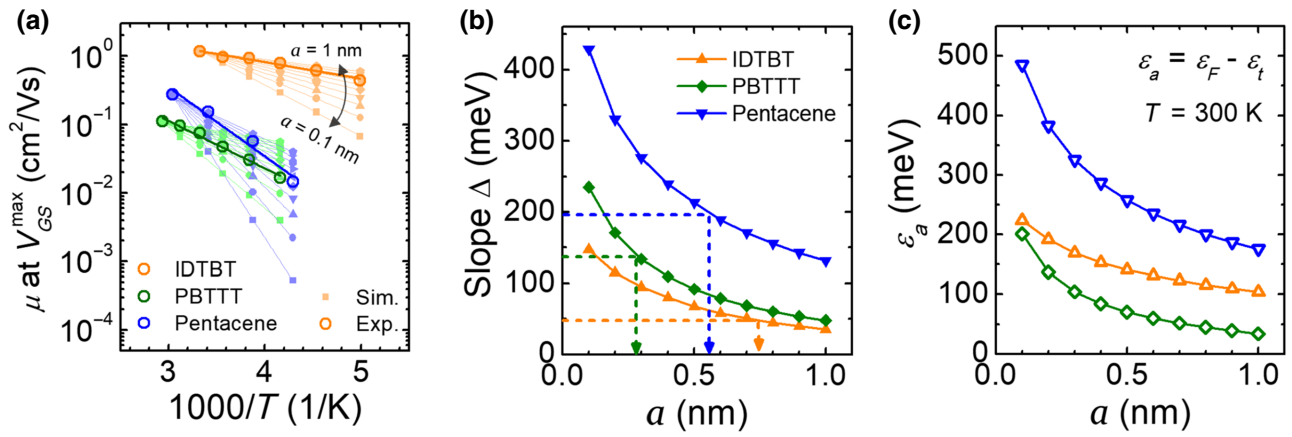


FIG. 5. (a) Experimentally measured and numerically calculated Arrhenius plots for IDTBT, PBTTT, and pentacene. Calculation considers $\sigma = 0.059$ eV, $N_0 = 7.4 \times 10^{20}$ cm⁻³, and $p/N_0 = 0.0126$ for IDTBT; $\sigma = 0.11$ eV, $N_0 = 8.9 \times 10^{20}$ cm⁻³, and $p/N_0 = 0.0243$ for PBTTT; and $\sigma = 0.15$ eV, $N_0 = 3 \times 10^{21}$ cm⁻³, and $p/N_0 = 3 \times 10^{-4}$ for pentacene. (b) Slopes of Arrhenius plot, Δ , with respect to a from (a). Horizontal and vertical dotted lines indicate Δ_{expt} and extracted a , respectively. (c) Direct calculation of $\epsilon_a = \epsilon_t - \epsilon_f$ using Eq. (3).

[18,20], does not mean ϵ_a of the SRGDM because the prefactor in Eq. (6) is not independent of T . According to our calculation, ϵ_t and $r(\epsilon_t)$ belong to the prefactor that varies with T .

According to the one-dimensional (1D) model by Nenashev *et al.*, it is the effective localization length, a_{eff} , that amounts to the molecular diameter, D , rather than the bare localization length, a_0 , (in the order of several Ångströms) [36]. According to the VRH transport model, the charge-carrier wave function penetrates not only into the adjacent molecules, but also into the more remote ones. In a three-dimensional (3D) system, a direct estimation of D is difficult because the molecular packing follows π - π stacking. In this case, the intermolecular distance (ID) along the π - π stacks can replace D . The calculated a is in fair agreement with the values of ID reported in the literature for all materials: 0.41 vs 0.75 nm for IDTBT [72], 0.38 vs 0.29 nm for PBTTT [73], and 0.4 vs 0.56 nm for pentacene [74]. For IDTBT, quasi-1D transport with occasional intermolecular

hopping through short π - π bridges occurs [75], so that the vertical ID [0.41 nm from grazing incidence x-ray scattering (GIXS) measurement of d spacing] is a determinant for a [Fig. 6(a)] [72]. For PBTTT, polymers stand edge-on on the substrate and two-dimensional (2D) transport takes place in the π - π stacking direction, so that the backbone's shortest length (0.38 nm from density-functional-theory calculations) corresponds to ID [Fig. 6(b)] [73]. For pentacene OFETs [Fig. 6(c)], molecules stand vertically on the insulator, so that charge carriers hop along the in-plane π - π stacking direction [76]. Therefore, assuming a 3D cuboid, the ID is around 0.4 nm [74].

We will now describe how localization length a affects the mobility via ϵ_t and the subsequent values of ϵ_a and $r(\epsilon_t)$ on the disordered system (Fig. 7). For all materials, ϵ_t becomes closer to ϵ_f as a increases [Fig. 7(a)], whereas $r(\epsilon_t)$ increases with an increase of a [Fig. 7(b)]. In this context, the origin of ϵ_t variation can be explained by the very physical definition of ϵ_t , that is, the energy

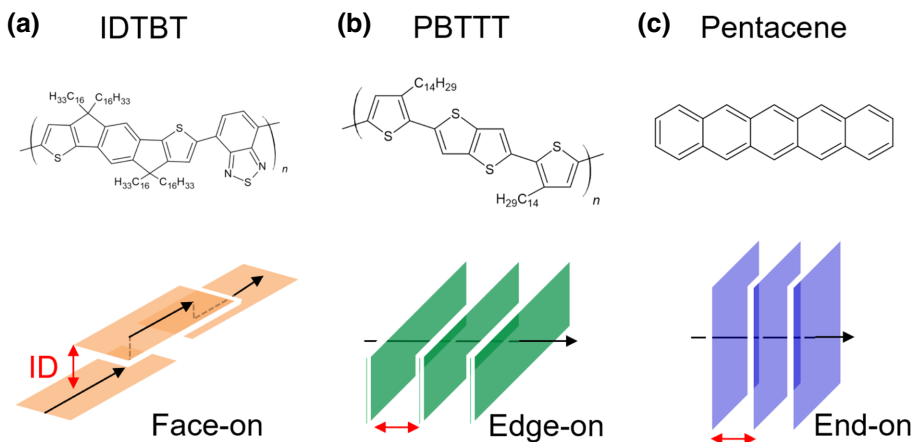


FIG. 6. Molecules and molecular orientation in thin films of (a) IDTBT, (b) PBTTT, and (c) pentacene. Black arrows indicate the direction of charge transport and red double-headed arrows indicate ID of π - π stacking.

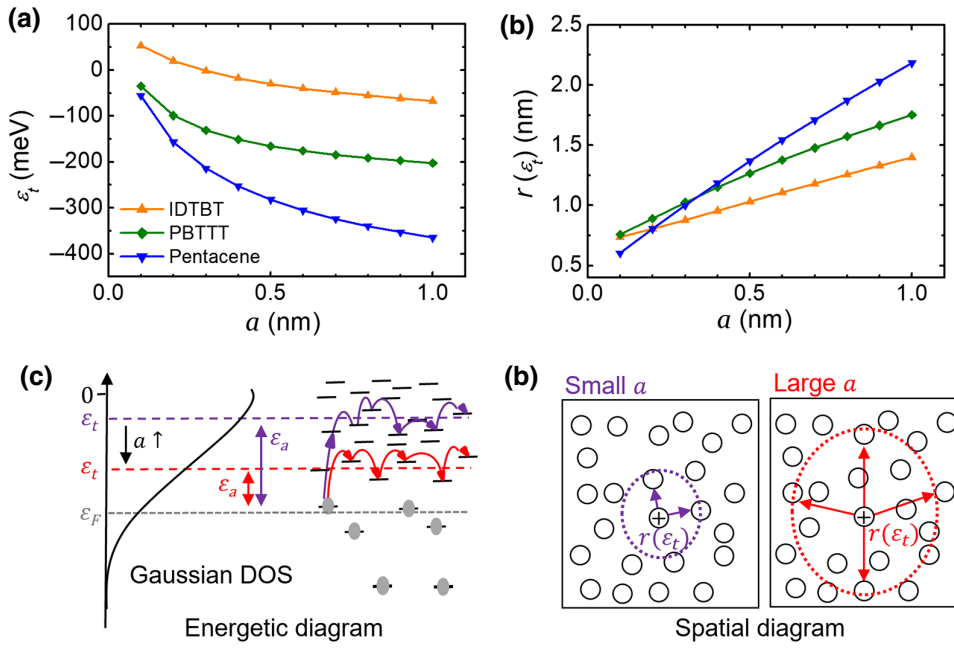


FIG. 7. Calculated results of (a) ε_t and (b) $r(\varepsilon_t)$ with respect to localization length a . Schematic illustration of the hopping range in (c) energetic and (d) spatial diagrams for different localization lengths a : small a in violet color; large a in red color.

that offers the fastest hopping transition rate for charge carriers [20]. When a is small, and hence, ε_t is close to HOMO_{\max} (0 eV), a charge carrier does not have sufficient states to hop for in the spatial domain due to the small $r(\varepsilon_t)$. Therefore, an energy that possesses a large number of neighboring states in the energetic domain is likely to be selected as ε_t to get the fastest upward-hopping transition rate. This mechanism can illustrate that ε_t is close to the center of the Gaussian DOS at small a . When a is large, ε_t prefers to be an energy that possesses small amounts of states because the system has enough states to hop in the spatial domain with a large $r(\varepsilon_t)$. Consequently, ε_t moves towards ε_F and the mobility increases when ε_a decreases.

At this stage, the localization length appears to be a prominent component for the parameterization of the SRGDM. In the next section, we discuss another obscure parameter, the attempt-to-escape frequency, for proper parameterization.

D. Attempt-to-escape frequency

In Fig. 5(a), the fitting of numerically calculated Arrhenius plots to experimental data at the highest temperature is used to estimate ν_0 for each material: $\nu_0 = 7.05 \times 10^{14} \text{ s}^{-1}$ for IDTBT ($a = 0.75 \text{ nm}$), $\nu_0 = 2.9 \times 10^{17} \text{ s}^{-1}$ for PBTTT ($a = 0.29 \text{ nm}$), and $\nu_0 = 6.76 \times 10^{16} \text{ s}^{-1}$ for pentacene ($a = 0.56 \text{ nm}$) [Fig. 8(a)]. A large ν_0 must be used to fit the experimental results. Notably, the extracted ν_0 values are up to three orders of magnitude higher than the literature values, $\nu_0 = 10^{12} - 10^{14} \text{ s}^{-1}$ [19,20,77].

We examine these extracted ν_0 values by comparing a direct calculation of the charge transition rate, ν_{ij} , from Eq. (2) to its theoretical estimation in the literature. If a value of ν_{ij} obtained through Eq. (2) from an obtained ν_0 is in the order of theoretical estimations of ν_{ij} , then this ν_0 would be physically sound. The value of ν_{ij} is calculated with the right-hand side of Eq. (2) for each ν_0 . The calculation considers $r(\varepsilon_t)$ in Eq. (4) to be r_{ij} and $\varepsilon_j = \varepsilon_t$, as

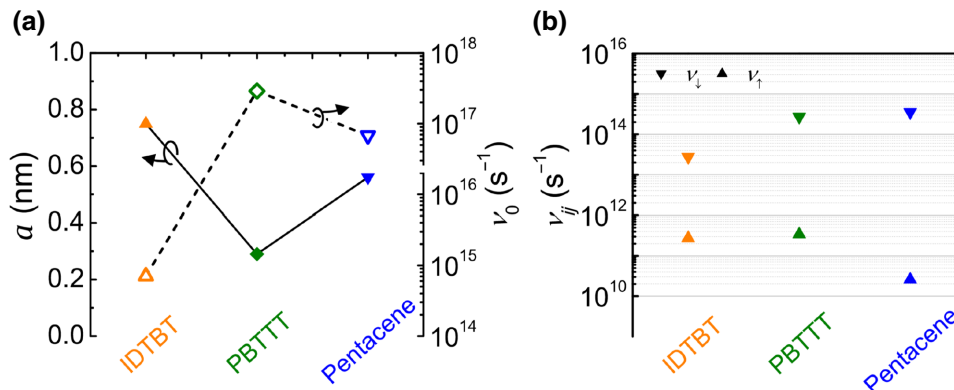


FIG. 8. (a) Extracted a and ν_0 from Fig. 5(a) for three different materials: IDTBT, PBTTT, and pentacene. (b) Direct calculation of MA upward, ν_{\uparrow} , and downward, ν_{\downarrow} , transition rates by Eq. (2) for each ν_0 from (a).

well as $\varepsilon_i = \varepsilon_F$ for upward hopping. Direct calculation of upward, ν_\uparrow , and downward, ν_\downarrow , transition rates with Eq. (2) are $\nu_\uparrow = 2.76 \times 10^{11} \text{ s}^{-1}$ and $\nu_\downarrow = 2.73 \times 10^{13} \text{ s}^{-1}$ for IDTBT, $\nu_\uparrow = 3.42 \times 10^{11} \text{ s}^{-1}$ and $\nu_\downarrow = 2.69 \times 10^{14} \text{ s}^{-1}$ for PBTBT, and $\nu_\uparrow = 2.58 \times 10^{10} \text{ s}^{-1}$ and $\nu_\downarrow = 3.51 \times 10^{14} \text{ s}^{-1}$ for pentacene [Fig. 8(b)]. Globally, ν_\downarrow are larger than ν_\uparrow because downward hops are independent of the energetic distribution of states, so that they are faster than upward hops.

For comparison with directly calculated ν_{ij} , theoretical estimations of ν_{ij} are conducted by MA and Marcus charge-transfer models [78]. Based on the MA transition rate, Bässler [68] stated that the small interaction energy between molecules induced by weak intermolecular coupling led to hopping transition rates between 10^{11} and 10^{13} s^{-1} . More recently, Brédas *et al.* calculated similar orders of energy rate in donor-acceptor pairs [69]. The Marcus model is another charge-transfer model for localized states that is compatible with the MA transition rate. Based on this theory, hole- and electron-transfer rates are calculated to be in the range between 10^{12} and 10^{13} s^{-1} in various organic disorder materials [79,80]. Remarkably, Nan *et al.* proved that the hole-transfer rates of rubrene, tetracene, and pentacene could reach up to

10^{14} s^{-1} when the quantum nuclear tunneling effect was considered [81].

Interestingly, the directly calculated values for ν_{ij} are in the range of the theoretical estimated values, in spite of their large magnitudes. This result illustrates that ν_0 can have a value of up to 10^{17} s^{-1} , depending on the materials, and these values are about four orders of magnitude higher than the conventionally reported values for GDMs. Notably, since ν_0 cannot be calculated, one should determine it from a comparison with experimental data. In this section, we have shown that predetermined a can facilitate the physically sound estimation of ν_0 for various materials.

IV. EXPERIMENTAL VALIDATION

A. Experimental data of OFETs

In this section, we validate the parametrization of the SRGDM by a comparison between the experimental results of IDTBT, PBTBT, and pentacene OFETs and the numerical TCAD simulation. The temperature evolutions of the transfer characteristics of IDTBT- and PBTBT-based [Figs. 9(a) and 9(b), symbols] top-gate staggered OFETs

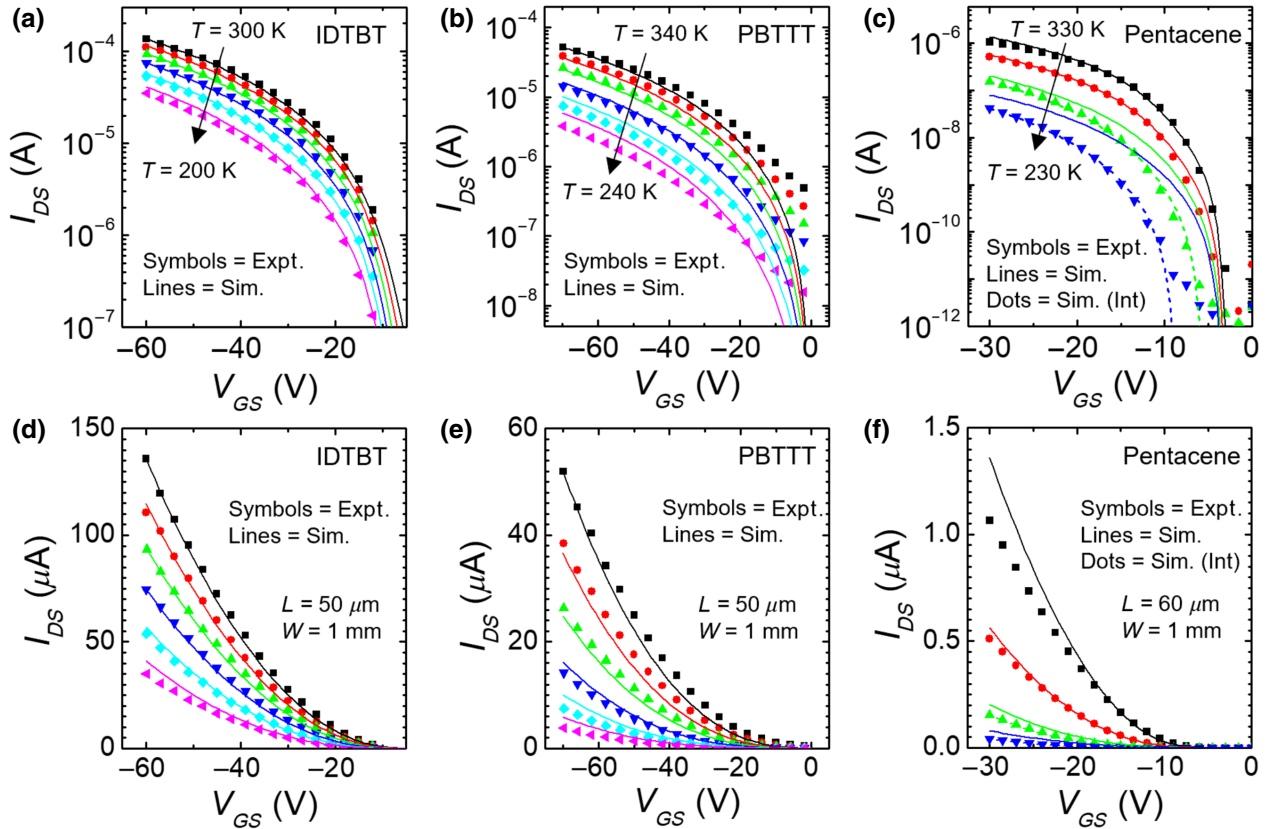


FIG. 9. Transfer curves on (a)–(c) semilogarithmic and (d)–(f) linear scales for IDTBT- ($V_{DS} = -60 \text{ V}$), PBTBT- ($V_{DS} = -70 \text{ V}$), and pentacene-based ($V_{DS} = -2 \text{ V}$) OFETs. Symbols illustrate measured data and solid lines show simulated results without interface trap states. For pentacene OFET, dotted lines for low temperatures, $T = 260$ and 230 K , represent simulated results with interface trap states. Channel length L and width W are indicated in the figure.

are taken from Venkateshvaran *et al.* [1]. The temperature is varied from 200 to 300 K for IDTBT and from 240 to 340 K for PBTTT at intervals of 20 K. For pentacene, a bottom-gate staggered OFET is fabricated. Details of the fabrication method are summarized in the Appendix. The temperature evolution of the transfer curves is measured under vacuum using a Keysight E5270B analyzer [Fig. 9(c), symbols]. A Janis cryostat is used to vary the temperature. Measurements are performed at $T = 330, 300, 260,$ and 230 K. The experimentally obtained drain current increases gradually as the temperature is increased for all OFETs because hopping transport is thermally assisted.

B. Numerical simulation of OFETs

To conduct a device-level simulation of the SRGDM, we implement the model into a TCAD simulator, ATLAS, from SILVAC. It calculates self-consistently the Poisson, continuity, and drift-diffusion equations based on a finite-element method, considering distinctive characteristics of ODSs, such as the Gaussian DOS, the generalized Einstein relation, and the SRGDM. The simulator calculates the transfer characteristics using the physical parameters of the fabricated devices (given in Table I), such as the device structures, and at various temperatures. In the simulation, the thermionic-emission model that describes the charge-carrier injection at the contact facilitated by temperature is not considered. The effective injection barrier, $E_b^{\text{eff}} = E_b - \sigma^2/(2kT)$, which considers the lowering of the injection barrier due to Gaussian disorder [82], of the devices is very small (0.18, -0.03 , and 0.36 eV for IDTBT,

PBTTT, and pentacene, respectively) and the corresponding contacts can be regarded as ohmic [83]. Therefore, the effect of temperature on the charge-carrier injection is negligible.

In several publications [84,85], it is shown that charge transport in OFETs is mainly of 2D character. A question might then arise of whether the concepts for the GDM formulated in 3D, such as the percolation factor and the transport energy, are applicable to charge transport in transistors with a small thickness of the transport channel. It should be emphasized that the 2D character of charge transport revealed in Refs. [84,85] does not mean that the thicknesses of the transport channel in OFETs is exactly zero. To answer the question about the applicability of 3D concepts, one has to compare the channel thickness with the characteristic length scale, $r(\epsilon_t)$, for hopping transport at the transport energy in 3D given by Eq. (4), multiplied by the percolation factor $B_C^{1/3}$, as expressed in Eq. (5). Taking typical values of $N_0 = 10^{21} \text{ cm}^{-3}$ and $\sigma = 4kT$, and using the value $B_C = 2.7$, from Eqs. (1), (3), and (4) one obtains the estimated $B_C^{1/3}$ and $r(\epsilon_t) \approx 1$ nm. The lowest experimental estimate of the channel thickness of about 5 nm [85] justifies, therefore, the applicability of 3D concepts for hopping transport. Furthermore, the charge density distribution in the transport channel calculated from the Poisson equation performed in Ref. [12] indicates a channel thickness of at least 10 nm. This value is much larger than the hopping length of 1 nm. Therefore, the 3D concepts are valid for a description of charge transport in OFETs.

TABLE I. Set of parameters used in the numerical simulation.

Categories	Parameters ^a	IDTBT	PBTTT	Pentacene	Unit
Device parameters	W_G	4.3	4.3	4.3	eV
	W_S and W_D	4.9	4.9	4.9	eV
	ϵ_i	2.1	2.2	2.5	...
	ϵ_s	3.5	1.55	4	...
	E_b	0.25	0.2	0.8	eV
GDM on random sites	N_0	7.4×10^{20}	8.9×10^{20}	3×10^{21}	cm^{-3}
	σ	0.059	0.11	0.15	eV
	a	0.75	0.29	0.56	nm
	ν_0	7.05×10^{14}	2.9×10^{17}	6.76×10^{16}	s^{-1}
	B_C	2.735	2.735	2.735	...
Donorlike bulk trap states	$N_{d,\text{bulk}}$	4×10^{14}	...	1×10^{15}	cm^{-3}
	$\sigma_{d,\text{bulk}}$	0.059	...	0.15	eV
	$E_{d,\text{bulk}}$	0.28	...	0.8	eV
Donorlike interface trap states	$N_{d,\text{int}}$ at 260 K	8×10^8	cm^{-2}
	$N_{d,\text{int}}$ at 230 K	1.8×10^9	cm^{-2}
	$\sigma_{d,\text{int}}$	0.15	eV
	$E_{d,\text{int}}$	1.1	eV

^a W_G , work function of gate electrode; W_S and W_D , work function of source and drain electrode; ϵ_i , dielectric constant of gate insulator; ϵ_s , dielectric constant of semiconductor; E_b , injection barrier from W_{SD} to HOMO_{max} ; N_d , trap density; σ_d , Gaussian width of trap Gaussian DOS; and E_d , energetic distance between intrinsic DOS and trap DOS.

Numerically calculated transfer curves show excellent fits to experimental data at all temperatures with a single set of parameters in both logarithmic [Figs. 9(a)–9(c), solid lines] and linear [Figs. 9(d)–9(f), solid lines] scales (Table I). The parameters consist of five physical parameters of the SRGDM (Fig. 1), device parameters, and secondary Gaussian trap states. The values for σ , a , and ν_0 are adopted from extracted values (Secs. IIIA, C, and D). Parameters such as N_0 [1,86]; the dielectric constant of the semiconductor, ϵ_s [87–89]; and the percolation constant, B_c [20,44] are taken from the literature. Simulations of IDTBT- and pentacene-based OFETs adopt Gaussian-distributed donorlike bulk trap states by the double Gaussian DOS model to consider the trap states [90], which lead to a better fit. The trap DOS widths, $\sigma_{d,\text{bulk}}$, are taken to be identical to σ of the HOMO. The volumetric bulk trap density, $N_{d,\text{bulk}}$, is in the typical range of an unintentional doping level [89]. Lastly, $E_{d,\text{bulk}}$ is determined by systematic simulations. Notably, we assume that Gaussian bulk trap states are invariable with temperature.

For pentacene OFETs at low temperature, the numerical simulation is not successful for fitting the measured transfer curves, despite consideration of the bulk trap states [Fig. 9(c), solid lines]. This deviation is attributed to the additional interface trap states between the semiconductor and gate insulator. At low temperature, the mismatch of thermal strain between the semiconductor and gate insulator can induce trap states at the interface [91]. According to universal scaling between the slope of the Arrhenius plot of mobility Δ and interfacial thermal expansion mismatch (ITEM) by Mei *et al.* [91], $\Delta_{\text{exptl.}} = 199.4\text{meV}$ (pentacene) indicates $\text{ITEM} \approx 650$, whereas $\Delta_{\text{exptl.}} = 137.5\text{meV}$ (PBTTT) and $\Delta_{\text{exptl.}} = 48.1\text{meV}$ (IDTBT) indicate $\text{ITEM} \approx 140$ and 13, respectively. Because the interface trap density is proportional to ITEM, the effect of the interface trap states is particularly apparent in the pentacene-based OFET. To consider the interface trap states, numerical calculations consider the Gaussian-shaped interface trap states at the interface between the semiconductor and gate insulator in addition to the bulk trap states. The order of areal interface trap density, $N_{d,\text{int}}$, is determined from the areal molecular density, $4.8 \times 10^{14} \text{cm}^{-2}$, and the ratio between N_0 and $N_{d,\text{bulk}}$. Then, $\sigma_{d,\text{int}}$ and $E_{d,\text{int}}$ are determined in a similar manner to that of the bulk trap states. At low temperature, the numerical calculation shows a good fit to measured data of the pentacene-based OFET [Fig. 9(c), dotted lines]. At high temperature ($T = 330 \text{K}$), however, the numerical result is slightly higher than the experimental result at a high V_{GS} on the linear scale [Fig. 9(f), black line]. This result could originate from mobility degradation due to charge-carrier scattering by the interface trap states, which becomes more dominant at high temperature and V_{GS} [92]. Since this mobility degradation mechanism is not considered in the numerical simulation, the calculated

current is slightly overestimated compared with the measured current.

V. CONCLUSIONS

The emphasis in our study is put on the replacement of simulation algorithms based previously on lattice models with only energy disorder in the simulation algorithms, which also take spatial disorder into account. This goal is dictated by the fact that the set of material parameters responsible for charge transport in spatially disordered systems is at variance with the set of material parameters responsible for charge transport in lattices. The GDM is considered in our study as a prototypical system.

An advanced parameterization of the GDM on spatially random sites is suggested. For ODSs with various degrees of disorder, the localization length and the attempt-to-escape frequency are extracted from the Arrhenius plots of the calculated and measured mobilities. The effects of the localization length on transport energy, activation energy, and hopping distance in the system with both spatial and energetic disorder are clarified. Remarkably, it is shown that the localization length has a similar order of magnitude to the intermolecular distance of the semiconductor along the π - π stacking direction. In addition, the attempt-to-escape frequency must be elevated up to the range of $10^{14} - 10^{17} \text{s}^{-1}$, depending on the materials, maintaining the calculated charge-transition rate within the physically accepted range. The sets of parameters enable an accurate fit of the transfer curves of various OFETs over a wide range of temperatures. We expect that this improvement in the theoretical tool will facilitate further improvement and correct evaluation of the device performance.

The model itself will probably also need an improvement by considering the possible correlations between the spatial disorder and the energy disorder, which is missing in the conventional GDM approach exploited in our study. While such correlations are reported for small-molecular ODSs, more research is needed to answer the question of whether the GDM is adequately applicable to describe charge transport in polymers, or whether this model should be extended by taking into account correlations between spatial disorder and energy disorder.

ACKNOWLEDGMENTS

This work is supported by a PhD fellowship from the École doctorale de l'Institut Polytechnique de Paris (ED IP Paris) and by the Basic Science Research Program through the National Research Foundation of Korea (NRF) funded by the Ministry of Education (Grant No. NRF-2018R1D1A1B07048877). Financial support of the key profile area “Quantum Matter and Materials (QM2)” at the University of Cologne and that of the Deutsche Forschungsgemeinschaft (Grant No. TG2591) is gratefully

acknowledged. Low-temperature current-voltage experiments are performed in the NanoMat' facility in Reims, supported by the Region Champagne-Ardenne, URCA, DRRT Grand Est, and FEDER programs.

APPENDIX: FABRICATION METHOD FOR PENTACENE OFET

The pentacene OFET is fabricated in a bottom-gate staggered structure with a channel length $L = 60 \mu\text{m}$ and channel width $W = 1 \text{ mm}$. Initially, the glass substrate is cleaned with acetone, isopropanol, and UV-ozone treatment, and then Al (100 nm) is thermally evaporated for the gate electrode. As for the gate insulator, polymethyl methacrylate (PMMA, MW = 120 000) is spin-coated for 600 nm on the Al/glass substrate. Lastly, pentacene (60 nm) and Au (30 nm) are thermally evaporated for the organic active layer and the source/drain electrode, respectively. Evaporation rates of both pentacene and Au are globally kept at 0.01 nm/s under 1.9×10^{-7} mbar. All processes, except cleaning, are carried out in a nitrogen glovebox. The remaining fabrication processes are identical to those reported in the literature [12,93].

-
- [1] D. Venkateshvaran, M. Nikolka, A. Sadhanala, V. Lemaire, M. Zelazny, M. Kepa, M. Hurhangee, A. J. Kronemeijer, V. Pecunia, I. Nasrallah, I. Romanov, K. Broch, I. McCulloch, D. Emin, Y. Olivier, J. Cornil, D. Beljonne, and H. Sirringhaus, Approaching disorder-free transport in high-mobility conjugated polymers, *Nature* **515**, 384 (2014).
- [2] Y. Hu, G. Li, W. Peng, and Z. Chen, Comparing the gate dependence of contact resistance and channel resistance in organic field-effect transistors for understanding the mobility overestimation issue, *IEEE Electron Device Lett.* **39**, 421 (2018).
- [3] Y. Lee, J. Kwon, S. Jung, W. Kim, S. Baek, and S. Jung, Reliable inkjet contact metallization on printed polymer semiconductors for fabricating staggered TFTs, *Appl. Phys. Lett.* **116**, 153301 (2020).
- [4] G. Wang, J. Swensen, D. Moses, and A. J. Heeger, Increased mobility from regioregular poly(3-hexylthiophene) field-effect transistors, *J. Appl. Phys.* **93**, 6137 (2003).
- [5] D. Boudinet, M. Benwadih, Y. Qi, S. Altazin, J. M. Verilhac, M. Kroger, C. Serbutoviez, R. Gwoziecki, R. Coppard, G. Le Blevenec, A. Kahn, and G. Horowitz, Modification of gold source and drain electrodes by self-assembled monolayer in staggered n- and p-channel organic thin film transistors, *Org. Electron.* **11**, 227 (2010).
- [6] C. Tanase, P. W. M. Blom, D. M. De Leeuw, and E. J. Meijer, Charge carrier density dependence of the hole mobility in poly(p-phenylene vinylene), *Phys. Status Solidi* **201**, 1236 (2004).
- [7] C. A. Amorim, M. R. Cavallari, G. Santos, F. J. Fonseca, A. M. Andrade, and S. Mergulhão, Determination of carrier mobility in MEH-PPV thin-films by stationary and transient current techniques, *J. Non. Cryst. Solids* **358**, 484 (2012).
- [8] S. Shaked, S. Tal, Y. Roichman, A. Razin, S. Xiao, Y. Eichen, and N. Tessler, Charge density and film morphology dependence of charge mobility in polymer field-effect transistors, *Adv. Mater.* **15**, 913 (2003).
- [9] G. Horowitz and M. E. Hajlaoui, Grain size dependent mobility in polycrystalline organic field-effect transistors, *Synth. Met.* **122**, 185 (2001).
- [10] B. Stadlober, M. Zirkl, M. Beutl, G. Leising, S. Bauer-Gogonea, and S. Bauer, High-mobility pentacene organic field-effect transistors with a high-dielectric-constant fluorinated polymer film gate dielectric, *Appl. Phys. Lett.* **86**, 242902 (2005).
- [11] G. Horowitz, P. Lang, M. Mottaghi, and H. Aubin, Extracting parameters from the current-voltage characteristics of organic field-effect transistors, *Adv. Funct. Mater.* **14**, 1069 (2004).
- [12] S. Jung, J. W. Jin, V. Mosser, Y. Bonnassieux, and G. Horowitz, A compact model and parameter extraction method for a staggered OFET with power-law contact resistance and mobility, *IEEE Trans. Electron Devices* **66**, 4894 (2019).
- [13] C. H. Kim, Y. Bonnassieux, G. Horowitz, and S. Member, Charge distribution and contact resistance model for coplanar organic field-effect transistors, *IEEE Trans. Electron Devices* **60**, 280 (2013).
- [14] L. Dunn and A. Dodabalapur, Temperature dependent transient velocity and mobility studies in an organic field effect transistor, *J. Appl. Phys.* **107**, 113714 (2010).
- [15] K. Ryu, I. Kymissis, V. Bulović, and C. G. Sodini, Direct extraction of mobility in pentacene OFETs using C-V and I-V measurements, *IEEE Electron Device Lett.* **26**, 716 (2005).
- [16] C. H. Kim, H. Hlaing, M. M. Payne, K. G. Yager, Y. Bonnassieux, G. Horowitz, J. E. Anthony, and I. Kymissis, Strongly correlated alignment of fluorinated 5,11-Bis(triethylgermylethynyl)anthradithiophene crystallites in solution-processed field-effect transistors, *ChemPhysChem* **15**, 2913 (2014).
- [17] G. Horowitz, R. Hajlaoui, H. Bouchriha, R. Bourguiga, and M. Hajlaoui, Concept of "threshold voltage" in organic field-effect transistors, *Adv. Mater.* **10**, 923 (1998).
- [18] H. Bässler, Charge transport in disordered organic photoconductors a monte carlo simulation study, *Phys. Status Solidi B* **175**, 15 (1993).
- [19] W. F. Pasveer, J. Cottaar, C. Tanase, R. Coehoorn, P. A. Bobbert, P. W. M. Blom, M. De Leeuw, and M. A. J. Michels, Unified Description of Charge-Carrier Mobilities in Disordered Semiconducting Polymers, *Phys. Rev. Lett.* **94**, 206601 (2005).
- [20] S. D. Baranovskii, Theoretical description of charge transport in disordered organic semiconductors, *Phys. Status Solidi* **251**, 487 (2014).
- [21] P. M. Borsenberger, E. H. Magin, M. Der Van Auweraer, and F. C. De Schryver, The role of disorder on charge transport in molecularly doped polymers and related materials, *Phys. Status Solidi* **140**, 9 (1993).
- [22] H. H. Fong and S. K. So, Effects of tertiary butyl substitution on the charge transporting properties of rubrene-based films, *Chem. Phys.* **298**, 119 (2004).
- [23] A. M. Ballantyne, L. Chen, J. Dane, T. Hammant, F. M. Braun, M. Heeney, W. Duffy, I. McCulloch, D.

- D. C. Bradley, and J. Nelson, The effect of poly(3-hexylthiophene) molecular weight on charge transport and the performance of polymer: Fullerene solar cells, *Adv. Funct. Mater.* **18**, 2373 (2008).
- [24] T. Upreti, Y. Wang, H. Zhang, D. Scheunemann, F. Gao, and M. Kemerink, Experimentally Validated Hopping-Transport Model for Energetically Disordered Organic Semiconductors, *Phys. Rev. Appl.* **12**, 064039 (2019).
- [25] S. L. M. Van Mensfoort, S. I. E. Vulto, R. A. J. Janssen, and R. Coehoorn, Hole transport in polyfluorene-based sandwich-type devices: Quantitative analysis of the role of energetic disorder, *Phys. Rev. B* **78**, 085208 (2008).
- [26] S. L. M. Van Mensfoort and R. Coehoorn, Effect of Gaussian disorder on the voltage dependence of the current density in sandwich-type devices based on organic semiconductors, *Phys. Rev. B* **78**, 085207 (2008).
- [27] S. Scheinert and G. Paasch, Influence of the carrier density in disordered organics with Gaussian density of states on organic field-effect transistors, *J. Appl. Phys.* **115**, 044507 (2014).
- [28] J. Kwon, S. Jung, Y. H. Kim, and S. Jung, Bistaggered contact geometry for symmetric dual-gate organic TFTs, *IEEE Trans. Electron Devices* **66**, 3118 (2019).
- [29] G. Horowitz, X. Peng, D. Fichou, and F. Garnier, The oligothiophene-based field-effect transistor: How It works and How to improve It, *J. Appl. Phys.* **67**, 528 (1990).
- [30] S. Jung, J. Kwon, S. Tokito, G. Horowitz, Y. Bonnassieux, and S. Jung, Compact modelling and SPICE simulation for three-dimensional, inkjet-printed organic transistors, inverters and ring oscillators, *J. Phys. D: Appl. Phys.* **52**, 444005 (2019).
- [31] S. D. Baranovskii, Mott lecture: Description of charge transport in disordered organic semiconductors: Analytical theories and computer simulations, *Phys. Status Solidi Appl. Mater. Sci.* **215**, 1700676 (2018).
- [32] Silvaco Inc., Atlas Ver. 5.14.0.R (2016).
- [33] Fluxim AG, SETFOS Simulation Software Setfos Version 4, Fluxim AG (2019).
- [34] B. I. Shklovskii, Hopping conduction in semiconductors subjected to a strong electric field, *Sov. Phys. Semicond.* **6**, 1964 (1973).
- [35] B. Baumeier, O. Stenzel, C. Poelking, D. Andrienko, and V. Schmidt, Stochastic modeling of molecular charge transport networks, *Phys. Rev. B* **86**, 184202 (2012).
- [36] A. V. Nenashev, J. O. Oelerich, and S. D. Baranovskii, Theoretical tools for the description of charge transport in disordered organic semiconductors, *J. Phys. Condens. Matter* **27**, 093201 (2015).
- [37] J. O. Oelerich, A. V. Nenashev, A. V. Dvurechenskii, F. Gebhard, and S. D. Baranovskii, Field dependence of hopping mobility: Lattice models against spatial disorder, *Phys. Rev. B* **96**, 195208 (2017).
- [38] A. V. Nenashev, J. O. Oelerich, A. V. Dvurechenskii, F. Gebhard, and S. D. Baranovskii, Fundamental characteristic length scale for the field dependence of hopping charge transport in disordered organic semiconductors, *Phys. Rev. B* **96**, 035204 (2017).
- [39] J. O. Oelerich, D. Huemmer, and S. D. Baranovskii, How to Find out the Density of States in Disordered Organic Semiconductors, *Phys. Rev. Lett.* **108**, 226403 (2012).
- [40] S. Marianer and B. I. Shklovskii, Effective temperature of hopping electrons in a strong electric field S, *Phys. Rev. B* **46**, 13100 (1992).
- [41] Silvaco Inc., Atlas Ver. 5.30.0.R (2020).
- [42] R. Coehoorn, W. F. Pasveer, P. A. Bobbert, and M. A. J. Michels, Charge-carrier concentration dependence of the hopping mobility in organic materials with Gaussian disorder, *Phys. Rev. B* **72**, 155206 (2005).
- [43] S. D. Baranovskii, T. Faber, F. Hensel, and P. Thomas, The applicability of the transport-energy concept to various disordered materials, *J. Phys. Condens. Matter* **9**, 2699 (1997).
- [44] C. D. Lorenz and R. M. Ziff, Precise determination of the critical percolation threshold for the three-dimensional “Swiss cheese” model using a growth algorithm, *J. Chem. Phys.* **114**, 3659 (2001).
- [45] J. O. Oelerich, F. Jansson, A. V. Nenashev, F. Gebhard, and S. D. Baranovskii, Energy position of the transport path in disordered organic semiconductors, *J. Phys. Condens. Matter* **26**, 255801 (2014).
- [46] Y. Roichman and N. Tessler, Generalized einstein relation for disordered semiconductors - implications for device performance, *Appl. Phys. Lett.* **80**, 1948 (2002).
- [47] S. D. Baranovskii, H. Cordes, F. Hensel, and G. Leising, Charge-carrier transport in disordered organic solids, *Phys. Rev. B* **62**, 7934 (2000).
- [48] O. Rubel, S. D. Baranovskii, P. Thomas, and S. Yamasaki, Concentration dependence of the hopping mobility in disordered organic solids, *Phys. Rev. B* **69**, 014206 (2004).
- [49] Z. G. Yu, D. L. Smith, A. Saxena, R. L. Martin, and A. R. Bishop, Molecular Geometry Fluctuation Model for the Mobility of Conjugated Polymers, *Phys. Rev. Lett.* **84**, 721 (2000).
- [50] M. Bouhassoune, S. L. M. van Mensfoort, P. A. Bobbert, and R. Coehoorn, Carrier-density and field-dependent charge-carrier mobility in organic semiconductors with correlated Gaussian disorder, *Org. Electron.* **10**, 437 (2009).
- [51] S. L. M. Van Mensfoort, V. Shabro, R. J. De Vries, R. A. J. Janssen, and R. Coehoorn, Hole transport in the organic small molecule material α -NPD: Evidence for the presence of correlated disorder, *J. Appl. Phys.* **107**, 113710 (2010).
- [52] C. Reese and Z. Bao, Detailed characterization of contact resistance, gate-bias-dependent field-effect mobility, and short-channel effects with microscale elastomeric single-crystal field-effect transistors, *Adv. Funct. Mater.* **19**, 763 (2009).
- [53] V. Podzorov, S. E. Sysoev, E. Loginova, V. M. Pudalov, and M. E. Gershenson, Single-crystal organic field effect transistors with the hole mobility ~ 8 cm²/Vs, *Appl. Phys. Lett.* **83**, 3504 (2003).
- [54] E. G. Bittle, J. I. Basham, T. N. Jackson, O. D. Jurchescu, and D. J. Gundlach, Mobility overestimation Due to gated contacts in organic field-effect transistors, *Nat. Commun.* **7**, 10908 (2016).
- [55] Y. Hu, Direct observation of the dipole-induced energetic disorder in rubrene single-crystal transistors by scanning kelvin probe microscopy, *J. Phys. Chem. Lett.* **9**, 2869 (2018).

- [56] S. Machida, Y. Nakayama, S. Duhm, Q. Xin, A. Funakoshi, N. Ogawa, S. Kera, N. Ueno, and H. Ishii, Highest-Occupied-molecular-orbital Band Dispersion of Rubrene Single Crystals as Observed by Angle-Resolved Ultraviolet Photoelectron Spectroscopy, *Phys. Rev. Lett.* **104**, 156401 (2010).
- [57] V. Lemaire, J. Cornil, R. Lazzaroni, H. Sirringhaus, D. Beljonne, and Y. Olivier, Resilience to conformational fluctuations controls energetic disorder in conjugated polymer materials: Insights from atomistic simulations, *Chem. Mater.* **31**, 6889 (2019).
- [58] N. Lu, L. Li, and M. Liu, Polaron effect and energetic disorder dependence of seebeck coefficient in organic transistors, *Org. Electron.* **16**, 113 (2015).
- [59] S. Barard, Time-of-Flight Charge Transport Studies on Triarylamine and Thiophene Based Polymers, *Unpublished PhD Thesis, Queen Mary University of London* (2009).
- [60] A. Vollmer, O. D. Jurchescu, I. Arfaoui, I. Salzmann, T. T. M. Palstra, P. Rudolf, J. Niemax, and J. Pflaum, The effect of oxygen exposure on pentacene electronic structure, **343**, 339 (2005).
- [61] S. Yogev, E. Halpern, R. Matsubara, M. Nakamura, and Y. Rosenwaks, Direct measurement of density of states in pentacene thin film transistors, *Phys. Rev. B* **84**, 165124 (2011).
- [62] H. L. Kwok, Hole mobility in structurally-different pentacene field-effect transistors, *ECS Trans.* **3**, 263 (2006).
- [63] I. G. Hill, J. Hwang, A. Kahn, C. Huang, J. E. McDermott, and J. Schwartz, Energy level alignment between 9-phosphonoanthracene self-assembled monolayers and pentacene, *Appl. Phys. Lett.* **90**, 9 (2007).
- [64] S. Hood, N. Zarrabi, P. Meredith, I. Kassal, and A. Armin, Measuring energetic disorder in organic semiconductors using the photogenerated charge-separation efficiency, *J. Phys. Chem. Lett.* **10**, 3863 (2019).
- [65] J. Tsurumi, H. Matsui, T. Kubo, R. Häusermann, C. Mitsui, T. Okamoto, S. Watanabe, and J. Takeya, Coexistence of ultra-long spin relaxation time and coherent charge transport in organic single-crystal semiconductors, *Nat. Phys.* **13**, 994 (2017).
- [66] J. Zhou, Y. C. Zhou, J. M. Zhao, C. Q. Wu, X. M. Ding, and X. Y. Hou, Carrier density dependence of mobility in organic solids: A monte carlo simulation, *Phys. Rev. B* **75**, 153201 (2007).
- [67] W. D. Gill, Drift mobilities in amorphous charge-transfer complexes of trinitrofluorenone and poly-n-vinylcarbazole, *J. Appl. Phys.* **43**, 5033 (1972).
- [68] H. Bässler, Localized states and electronic transport in single component organic solids with diagonal disorder, *Phys. Status Solidi* **107**, 9 (1981).
- [69] J.-L. Bredas, D. Beljonne, V. Coropceanu, and J. Cornil, Charge-transfer and energy-transfer processes in π -conjugated oligomers and polymers: A molecular picture *Chem. Rev.* **104**, 4971 (2004).
- [70] A. Miller and E. Abrahams, Impurity conduction at Low concentrations, *Phys. Rev.* **120**, 745 (1960).
- [71] V. Ambegaokar, B. I. Halperin, and J. S. Langer, Hopping conductivity in disordered systems, *Phys. Rev. B* **4**, 2612 (1971).
- [72] W. Zhang, J. Smith, S. E. Watkins, R. Gysel, M. McGehee, A. Salleo, J. Kirkpatrick, S. Ashraf, T. Anthopoulos, M. Heeney, and I. McCulloch, Indacenodithiophene semiconducting polymers for high-performance, Air-stable transistors, *J. Am. Chem. Soc.* **132**, 11437 (2010).
- [73] D. M. DeLongchamp, R. J. Kline, E. K. Lin, D. A. Fischer, L. J. Richter, L. A. Lucas, M. Heeney, I. McCulloch, and J. E. Northrup, High carrier mobility polythiophene thin films: Structure determination by experiment and theory, *Adv. Mater.* **19**, 833 (2007).
- [74] R. B. Campbell, J. Monteath Robertson, and J. Trotter, The crystal and molecular structure of pentacene, *Acta Cryst.* **14**, 705 (1961).
- [75] X. Zhang, H. Bronstein, A. J. Kronemeijer, J. Smith, Y. Kim, R. J. Kline, L. J. Richter, T. D. Anthopoulos, H. Sirringhaus, K. Song, M. Heeney, W. Zhang, I. McCulloch, and D. M. DeLongchamp, Molecular origin of high field-effect mobility in an indacenodithiophene- benzothiadiazole copolymer, *Nat. Commun.* **4**, 2238 (2013).
- [76] W. H. Lee, J. Park, S. H. Sim, S. Lim, K. S. Kim, B. H. Hong, and K. Cho, Surface-Directed molecular assembly of pentacene on monolayer graphene for high-performance organic transistors, *J. Am. Chem. Soc.* **133**, 4447 (2011).
- [77] U. Siegner, D. Weber, E. O. Gobel, D. Binnhardt, V. Heuckeroth, R. Saleh, S. D. Baranovskii, P. Thomas, H. Schwab, C. Klingshirn, J. M. Hvam, and V. G. Lyssenko, Optical dephasing in semiconductor mixed crystals, *Phys. Rev. B* **46**, 4564 (1992).
- [78] R. A. Marcus, Electron transfer reactions in chemistry. theory and experiment, *Rev. Mod. Phys.* **65**, 559 (1993).
- [79] G. R. Hutchison, M. A. Ratner, and T. J. Marks, Intermolecular charge transfer between heterocyclic oligomers. effects of heteroatom and molecular packing on hopping transport in organic semiconductors, *J. Am. Chem. Soc.* **127**, 16866 (2005).
- [80] G. R. Hutchison, M. A. Ratner, and T. J. Marks, Hopping transport in conductive heterocyclic oligomers: Reorganization energies and substituent effects, *J. Am. Chem. Soc.* **127**, 2339 (2005).
- [81] G. Nan, X. Yang, L. Wang, Z. Shuai, and Y. Zhao, Nuclear tunneling effects of charge transport in rubrene, tetracene, and pentacene, *Phys. Rev. B* **79**, 115203 (2009).
- [82] S. Jung, C.-H. Kim, Y. Bonnassieux, and G. Horowitz, Injection barrier at metal/organic semiconductor junctions with a Gaussian density-of-states, *J. Phys. D: Appl. Phys.* **48**, 395103 (2015).
- [83] S. Jung, Y. Lee, A. Plews, A. Nejm, and Y. Bonnassieux, Effect of Gaussian disorder on power-law contact resistance and mobility in organic field-effect transistors, *IEEE Trans. Electron Devices* **68**, 307 (2020).
- [84] H. Sirringhaus, P. J. Brown, R. H. Friend, M. M. Nielsen, K. Bechgaard, B. M. W. Langeveld-Voss, A. J. H. Spiering, R. A. J. Janssen, E. W. Meijer, P. Herwig, and D. M. de Leeuw, Two-Dimensional charge transport in conjugated polymers, *Nature* **401**, 685 (1999).
- [85] A. Dodabalapur, L. Torsi, and H. E. Katz, Organic transistors: Two-dimensional transport and improved electrical characteristics, *Science* **268**, 270 (1995).
- [86] D. V. Lang, X. Chi, T. Siegrist, A. M. Sergent, and A. P. Ramirez, Amorphouslike Density of Gap States in Single-Crystal Pentacene, *Phys. Rev. Lett.* **93**, 086802 (2004).

- [87] M. Nikolka, I. Nasrallah, B. Rose, M. K. Ravva, K. Broch, A. Sadhanala, D. Harkin, J. Charmet, M. Hurhangee, A. Brown, S. Illig, P. Too, J. Jongman, I. McCulloch, J. L. Bredas, and H. Sirringhaus, High operational and environmental stability of high-mobility conjugated polymer field-effect transistors through the Use of molecular additives, *Nat. Mater.* **16**, 356 (2017).
- [88] R. Porrazzo, S. Bellani, A. Luzio, C. Bertarelli, G. Lanzani, M. Caironi, and M. R. Antognazza, Field-Effect and capacitive properties of water-gated transistors based on polythiophene derivatives, *APL Mater.* **3**, 014905 (2015).
- [89] C. H. Kim, O. Yaghmazadeh, D. Tondelier, Y. Bin Jeong, Y. Bonnassieux, and G. Horowitz, Capacitive behavior of pentacene-based diodes: Quasistatic dielectric constant and dielectric strength, *J. Appl. Phys.* **109**, 083710 (2011).
- [90] V. I. Arkhipov, P. Heremans, E. V. Emelianova, G. J. Adriaenssens, and H. Bässler, Charge carrier mobility in doped disordered organic semiconductors, *J. Non. Cryst. Solids* **338–340**, 603 (2004).
- [91] Y. Mei, P. J. Diemer, M. R. Niazi, R. K. Hallani, K. Jarolimek, C. S. Day, C. Risko, J. E. Anthony, A. Amassian, and O. D. Jurchescu, Crossover from band-like to thermally activated charge transport in organic transistors Due to strain-induced traps, *Proc. Natl. Acad. Sci.* **114**, E6739 (2017).
- [92] A. Nigam, D. Kabra, T. Garg, M. Premaratne, and V. R. Rao, Insight into the charge transport and degradation mechanisms in organic transistors operating at elevated temperatures in Air, *Org. Electron.* **22**, 202 (2015).
- [93] S. Jung, M. Albariqi, G. Gruntz, T. Al Hathal, A. Peinado, E. Garcia-Caurel, Y. Nicolas, T. Toupance, Y. Bonnassieux, and G. Horowitz, A TIPS-TPDO-TetraCN-based n -type organic field-effect transistor with a cross-linked PMMA polymer gate dielectric, *ACS Appl. Mater. Interfaces* **8**, 14701 (2016).